Lithos 323 (2018) 91–102

Contents lists available at ScienceDirect

Lithos

journal homepage: www.elsevier.com/locate/lithos

Interaction of highly saline fluid and olivine gabbro: Experimental simulation of deep hydrothermal processes involving amphibole at the base of the oceanic crust

Adriana Currin [a,*], Juergen Koepke [a], Renat R. Almeev [a], Oliver Beermann [b]

[a] Leibniz Universität Hannover, Institut für Mineralogie, Callinstr. 3, Hannover D-30167, Germany
[b] Christian-Albrechts-Universität zu Kiel, Institut für Geowissenschaften, Ludewig-Meyn-Str. 10, Kiel D-24118, Germany

ARTICLE INFO

Article history:
Received 27 March 2018
Revised 8 September 2018
Accepted 12 September 2018

Keywords:
Magmatic-hydrothermal transition
High-temperature hydrothermal activity
Fluid/rock interaction
Cl-bearing amphibole
Lower oceanic crust
Experimental petrology

ABSTRACT

Natural occurrences of Cl-bearing amphibole indicate crystallization in the presence of a highly saline fluid. Amphibole with varying Cl contents (0.1 to 5 wt% Cl) found in lower oceanic crustal rocks demonstrates the activity of saline hydrothermal fluids at depth. Here we present an experimental study done in cold seal pressure vessels (CSPV) and internally heated pressure vessels (IHPV) to illustrate the process by which gabbro-hosted amphibole-rich parageneses evolve in the presence of a hydrothermal saline fluid. The starting material used was a natural gabbroic rock containing high-Ti magnesio-hastingsite with the addition of a moderately to highly saline fluid (NaCl-H_2O) with X_{NaCl} = 0.02, 0.07 and 0.24 (6, 20 and 50 wt% NaCl). We evaluated a range of conditions from hydrothermal (500–750 °C) to magmatic (900 °C) at pressures of 200 MPa and fO_2 close to NNO. Fluid/rock mass ratios used were 0.2 and 1 in subsolidus (hydrothermal) experiments, and 0.07 in partial melting (magmatic) experiments. New amphibole was formed on rims of the starting high-Ti magnesio-hastingsite, with product compositions corresponding to magnesio-hastingsite, high-Si magnesio-hornblende, tschermakite, edenite, hastingsite and ferro-pargasite with varying Cl contents up to 0.47 wt% Cl. Our results from subsolidus experiments demonstrate a decrease in olivine, plagioclase and clinopyroxene in the starting rock, and formation of new amphibole, with decreased ^{IV}Al and Ti with respect to starting amphibole. Product amphibole does not display any correlation between Cl and Fe^{2+}, ^{IV}Al and K, in contrast to natural highly Cl-rich amphibole, suggesting that these correlations hold true only at Cl contents higher than those attained in our experiments. In addition, we found that increasing NaCl in the fluid correlates with increased maximum Cl contents in amphibole. Compositional variations found in product amphibole highlight the heterogeneities in fluid infiltration and Cl activity that account for the complexity of hydrothermal fluid/rock interactions in deep oceanic geological systems.

1. Introduction

Volatile-bearing minerals such as amphibole can provide essential information on the interaction between fluids and rocks and contribute to our understanding of the cycling of volatiles and volatile budgets during geological processes (e.g., Filiberto and Treiman, 2009; Sautter et al., 2006; Taylor et al., 2010). In the oceanic crust – which covers two thirds of our planet – amphibole-bearing assemblages found in gabbros have the potential to provide information on the interaction record between seawater-derived fluids and rock down to the base of the crust near mid-ocean ridges (Manning et al., 1996; Coogan et al., 2001; Nicolas et al., 2003; Bosch et al., 2004; Silantyev et al., 2008; Aranovich et al., 2010; Silantyev et al., 2010; among others). Due to its large range of temperature stability, amphibole is able to record the evolution of hydrothermal systems from the magmatic regime, via the ductile-brittle transition at early stage formation of the oceanic crust (e.g., Bosch et al., 2004; Coogan et al., 2001) down to increased hydrothermal activity upon progressive brittle deformation in the greenschist and sub-greenschist facies (at temperatures above ca. 300 °C: Alt et al., 2010). Thermal models have shown that the hydrothermal system cooling the oceanic crust may reach lower crustal depths of about 6 km (Maclennan et al., 2005). Studies done on ophiolites associated to mid-ocean ridge systems can provide insight into processes occurring in the oceanic crust. For instance, Nicolas et al. (2003) describe the infiltration pathways of seawater into gabbros of the Samail ophiolite (Sultanate of Oman) down to the base of the crust and at about 1 km off the ridge axis. Hydrothermal alteration products of these gabbros are described by Bosch et al. (2004). These authors note that hydrothermal alteration occurred over a wide range of conditions, from very high temperatures at low water/rock ratios (3–5) at the transition between magmatic and metamorphic processes (>975 °C), down to 500 °C,

* Corresponding author.
E-mail address: a.currin@mineralogie.uni-hannover.de (A. Currin).

https://doi.org/10.1016/j.lithos.2018.09.017
0024-4937/

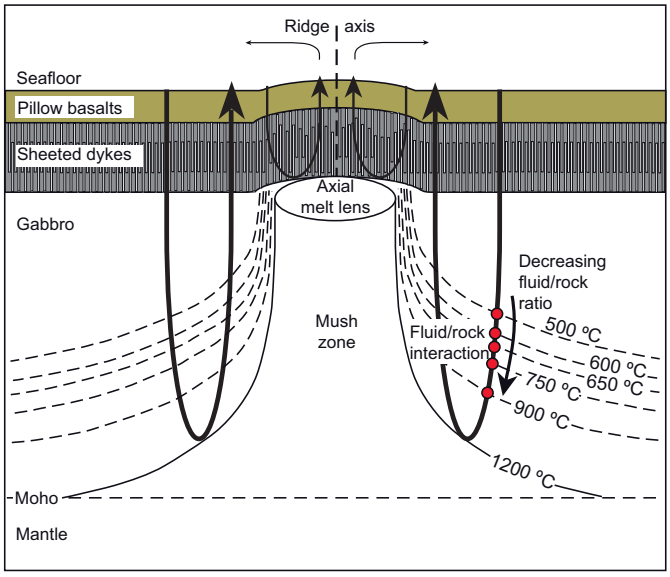

Fig. 1. Schematic cross-section of the oceanic crust below fast-spreading mid-ocean ridges showing seawater-derived fluid/rock interaction in the lower oceanic crust. Arrows indicate extent of hydrothermal systems (e.g. Gregory and Taylor, 1981; Nicolas et al., 2003). Dots illustrate the geological conditions simulated in the experiments presented in this work. Isotherms (dashed lines) are from Dunn et al., 2000. Not to scale.

well into the subsolidus regime at higher fluid/rock ratios (>10). Based on isotopic analyses, it was found that infiltration of the aforementioned hydrothermal fluids followed deep penetration of seawater (Bosch et al., 2004). However, a lower range of water/rock ratios for diversely altered oceanic gabbro has been determined: for the Semail ophiolite (≤ 0.3: Gregory and Taylor, 1981; 0.5 to 4.2: McCulloch et al., 1981), for Hess Deep, East Pacific Rise (0.2 to 1: Lecuyer and Reynard, 1996) or for the Mid-Cayman Ridge (0.2 to 1.7: Ito and Clayton, 1983).

1.1. Interaction of seawater-derived fluids with amphibole in oceanic rocks

Studies on the occurrence of Cl-rich amphibole in various types of low to high grade metamorphosed and hydrothermally altered rocks have led to the general conclusion that such phases interacted with highly saline fluids (e.g., Aranovich and Safonov, 2018; Enami et al., 1999; Kullerud, 1996; Léger et al., 1996; Liu et al., 2009; McCormick and McDonald, 1999; Morrison, 1991; Vanko, 1986). Changing fluid activity ratios ($a\mathrm{Cl}^-/a\mathrm{OH}^-$) and changes in fluid/rock ratios are reflected in variations of Cl content in amphibole in the presence of hydrothermal fluids (Kullerud, 2000). Seawater-derived fluids reaching the lower oceanic crust have already undergone many changes during their passage through the upper oceanic crust and have concentrated NaCl (Aranovich et al., 2010; Pertsev et al., 2015). When reaching the lower oceanic crust, amphibole preferentially takes up OH^- with respect to Cl^- from circulating hydrothermal fluids, contributing further to fluid salinity increase and fluid/rock ratio decrease (Aranovich et al., 2010; Coogan et al., 2001; Ito and Anderson, 1983; Kullerud, 1996; Kullerud, 2000; Silantyev et al., 2010). Cl-enrichment of hydrothermal fluids may occur in the deep oceanic crust, where high temperatures lead to boiling and concentration of solutes in the fluid, and fluid phase separation into low-Cl vapour and high-Cl liquid or brine (Aranovich et al., 2010).

The equilibration of amphibole with seawater-derived fluids may occur at different temperatures from suprasolidus to subsolidus conditions, at different stages of hydrothermal cooling of the oceanic crust (Fig. 1). Based on the thermometric study of samples from the Mid-Atlantic Ridge and the systematics between Cl, major element, trace element and rare-earth element compositions, Coogan et al. (2001) highlighted the importance of detecting Cl enrichment in lower crustal amphibole to discriminate between amphiboles formed in the suprasolidus regime from those formed in the subsolidus hydrothermal regime. Chlorine contents of amphibole formed in the deep oceanic crust may vary along a range from below several tenths of ppm (μg/g) to >5 wt% Cl, demonstrating variations in salinity of the reacting fluid (i.e. Vanko, 1986; Coogan et al., 2001; Silantyev et al., 2008; Wolff, 2014; Currin et al., 2018).

1.2. Previous work

This study is motivated by the finding of Cl-bearing amphibole with significant compositional variations in the layered gabbro section of the Oman Ophiolite (Currin et al., 2018). Fig. 2 shows the occurrence of magmatic zoned pargasite on the boundary between a layered olivine gabbro and a gabbroic dykelet, sampled in the vicinity of the crust/mantle boundary. The different compositional zones found within this pargasite grain are formed as a result of fluid/rock interaction at temperatures ranging from magmatic to hydrothermal (amphibolite facies). The different zones of this pargasite grain have different Cl contents ranging from <0.2 to >5 wt% Cl, as well as different cation compositions. Compositional variations between zones reflect changes in the reacting hydrothermal fluid, such as water/rock ratio, Cl content, and temperature. Further details on rocks sampled in Wadi Wariyah can be found in Currin et al. (2018).

Previous experimental studies documented in the literature have dealt with fluid/rock interaction in lower oceanic crustal environments, some including amphibole in starting or product assemblages, and in some cases involving Cl-rich brines or highly saline fluids. Koepke et al. (2004; 2007) and Wolff et al. (2013), conducted experiments in the supra-solidus regime involving hydrous partial melting triggered by a Cl-containing fluid to investigate the formation of plagiogranites using natural gabbroic rock as starting material and IHPV as in our study, but with a completely different aim. Sato et al. (2005) also used IHPV and, as in our study, investigated Cl-rich amphiboles, to find out the partition coefficient between Cl and melt in amphibole in volcanic settings (Sato et al., 2005). In the subsolidus regime, Grant and Harlov (2018) performed experiments applied to mafic rocks from the lower continental crust at amphibolite-granulite facies conditions and produced mildly Cl-bearing amphibole. On the other hand, Chan et al. (2016), and Mueller et al. (2017) used an experimental approach with synthetic starting compositions and formed highly Cl-rich amphiboles in the sub-solidus regime (>2 wt% Cl). Khodorevskaya and Aranovich (2016) studied the interaction between amphibole and highly saline

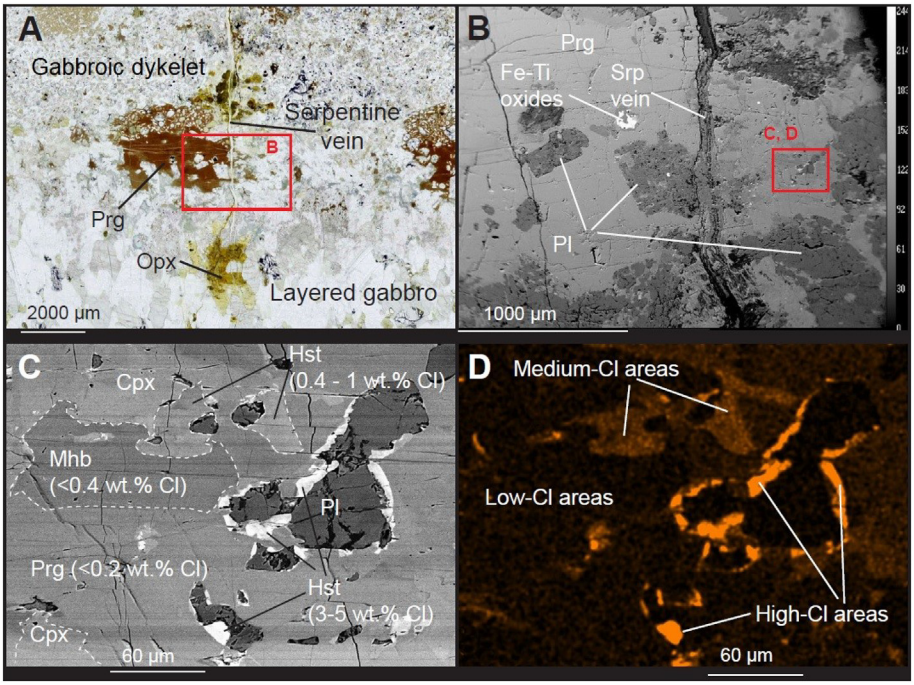

Fig. 2. A: Thin section microphotograph of sample WA32A, showing boundary between layered gabbro and a gabbroic dykelet. B: BSE images of the same area in more detail. C: Detail of alteration of pargasite and plagioclase to highly Cl-rich hastingsite, and magnesio-hornblende zone. D: Cl map produced by SEM/EDX of area C, brightness denotes high Cl contents, and dark areas are Cl-poor. Mineral abbreviations after Whitney and Evans (2010); Hst: hastingsite; Mhb: magnesio-hornblende; Prg: pargasite; Srp: serpentine; Pl: plagioclase; Opx: orthopyroxene; Cpx: clinopyroxene.

fluid at 900 °C, forming Cl-bearing amphiboles. Using a similar approach, but adding the context of the host rock by using natural solid rock starting materials and covering the whole range from suprasolidus to subsolidus conditions, the present study aims to investigate amphibole formation in gabbros of the lower oceanic crust by conducting both partial melting and hydrothermal experiments.

In this paper, we present an experimental simulation of the interaction of seawater-derived fluids with gabbroic rocks, in order to increase our understanding of the role of fluids in the alteration of the deep oceanic crust. Temperatures from 900 °C to 500 °C were applied, covering the interval from the partial molten state into the metamorphic regime down to greenschist facies conditions. The main focus of this study is the variations in cation content of amphibole, obtained in all experiments, as a function of temperature and fluid salinity. Due to our direct approach, using only gabbro and fluid as starting material at a pressure of 200 MPa, these experiments are highly relevant to natural fluid/rock interactions in the lower oceanic crust, and our results can thus be directly applied to nature (Fig. 1). An additional aspect of this study is to investigate the possibility of incorporation of Cl into the amphibole structure, as a response to experimental parameters, and to highlight the crystalchemical constraints for Cl substitution.

2. Experimental strategy and methods

In the present study, we aim to simulate the reactions producing a variety of amphibole compositions in the deep oceanic crust beneath mid-ocean ridges as a result of the interaction of aqueous NaCl-rich fluids and olivine gabbro. Experiments were conducted at 200 MPa, corresponding to pressures at the base of the oceanic crust at ~ 5 to 6 km depth for typical oceanic crust (Canales et al., 2003). Experimental temperatures (900, 750, 650, 600 and 500 °C) were chosen to simulate reactions during successive cooling of the lower oceanic crust, from magmatic, suprasolidus (900 °C) conditions, to hydrothermal, subsolidus conditions (750–500 °C), following the transition from granulite over amphibolite to greenschist facies conditions. The fluid/rock mass ratios selected were 0.07 (900 °C), 0.2 (750–650 °C) and 1 (600 and 500 °C), consistent with the concept of rock-dominated conditions (i.e. fluid/rock mass ratios lower than unity) during fluid interactions with dense, deep gabbro at high temperature, and the increasing influence of hydrothermal fluids with increasing extent of brittle deformation upon cooling (e.g., Bosch et al., 2004). To simulate an open system with increasing influence of hydrothermal activity at a particular temperature, an additional approach was used for experiments at 750 °C (experiments CSB50-2 and CSB20-2). The solid products from the first run (1) were retrieved from the capsule and half of the material was analysed, while the other half was run a second time (2) in a new capsule with a new batch of fluid of the same NaCl concentration and the same fluid/rock ratio (0.2) than in the first run. This procedure could potentially be reproduced multiple times to simulate repeated pulses of hydrothermal activity in the oceanic crust, however, experiments often result in comminution of the solid material and loss during opening of the capsules and transfer to a clean jar, which constrains the number of times this operation can be replicated and analysed successfully.

The geological setting corresponding to the experimental approach is illustrated in Fig. 1. As explained in the following section, the higher water/rock ratio (1) in hydrothermal experiments conducted at the lowest temperatures (600 and 500 °C) were intended to facilitate free growth of alteration minerals into the fluid and to attempt to reach conditions near to local fluid-mineral equilibrium. However, when employing coarse-grained starting minerals in the experimental capsule, particularly using a solid rock cylinder and not a powder, reaching equilibrium (global or local) is extremely difficult.

2.1. Starting material and sample preparation

In order to provide optimal conditions for the crystallization of amphibole, we used an olivine gabbro containing amphibole in its starting mineral assemblage, to serve as nucleation sites for new amphibole. The composition of the starting amphibole is unique, homogeneous, and easy to distinguish from product amphibole. The gabbro used is an amphibole-bearing gneissic olivine gabbro from the lower crust of the

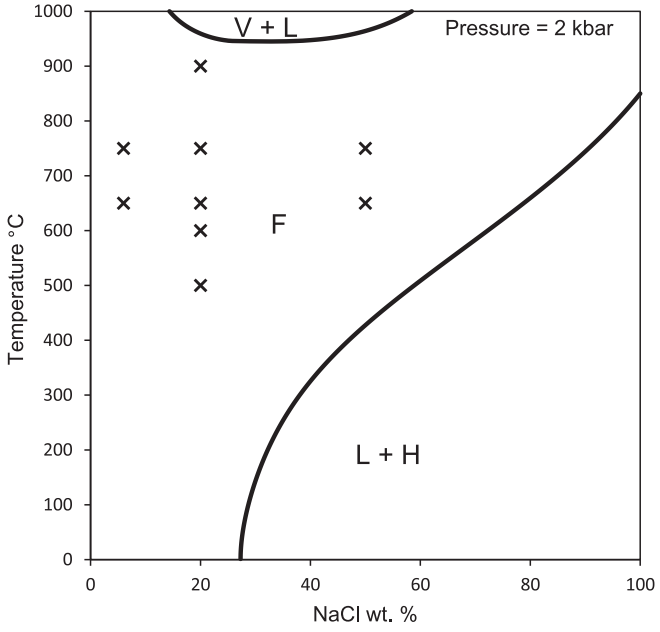

Fig. 3. Phase diagrams of the NaCl-H_2O system at 200 MPa. The different fields represented are: vapour and liquid (V + L), liquid and halite (L + H), and fluid (F), where – according to the terms used by Driesner and Heinrich (2007) – "F" denotes any type of fluid that can change properties from vapour to liquid-like without undergoing heterogeneous phase transitions. Experimental conditions shown by crosses. Curves calculated using the 'SoWat' model for fluid properties in the NaCl-H_2O system (Driesner, 2007; Driesner and Heinrich, 2007).

Mid-Atlantic Ridge near the Kane fracture zone, drilled by ODP during Leg 153 (Hole 920B, Core 13, Section 4, 32–36 cm) consisting of olivine, plagioclase, clinopyroxene, small amounts of orthopyroxene (<2 vol%), magnetite and Ti-rich magnesio-hastingsite in its original assemblage. This amphibole is of magmatic origin and extremely poor in Cl (<0.01 wt% Cl). Rock cylinders of the starting olivine gabbro were used for experiments (diameter 3.5 mm; height: 3.8 mm). For experiments at lower temperature (500 and 600 °C), larger cylinders of the same starting gabbro were used (7 mm in diameter and 10 mm in height). The aqueous starting solutions used ranged from moderately to highly saline with NaCl concentrations of 6, 20 and 50 wt% (0.02, 0.07 and 0.24 X_{NaCl}) and therefore ~2–16 times richer in Cl than seawater (~3.2 wt% NaCl; ~0.01 X_{NaCl}). These starting solutions were produced by dissolving reagent grade NaCl in distilled water in appropriate proportions – or by directly inserting NaCl crystals and water into the experimental capsule when using NaCl/water proportions (e.g. 50 wt% NaCl) exceeding NaCl saturation at ambient conditions. At the experimental pressure and temperature conditions used, all solutions were single phase fluids above critical pressure (Fig. 3) (Driesner, 2007; Driesner and Heinrich, 2007). The corresponding densities with respect to pure NaCl-H_2O fluids were calculated using the equations of Driesner (2007), ranging from 0.55 to 1.06 g/cm^3 (Table 1). Taking into account lower reaction kinetics expected from lower temperature experiments (500–600 °C), a longer run duration was chosen (101 days) to obtain secondary phases large enough for analysis (for details see Table 1).

Fluid and rock starting materials – and salt in experiments using 50 wt% NaCl – were weighed and inserted into capsules made of gold tubing with 0.1 mm wall thickness and inner diameter of 3.8 mm and 20 mm length or, for the longer cylinders, 0.2 mm wall thickness and 7.6 mm inner diameter and 50 mm length. The charged capsules were closed by pulsed electric arc welding under argon gas using a LAMPERT® PUK3 welding station. This method keeps the capsules cool during sealing to avoid evaporation of the charge. Capsules were then left in an oven at 110 °C for a few hours and subsequently weighed, to ensure they were properly sealed before proceeding to the experiments. For experimental details see Table 1.

2.2. Experimental apparatuses and procedure

All experiments were conducted at a pressure of 200 MPa in different kinds of pressure vessels. The single partial melting, suprasolidus experiment (900 °C) was conducted in an Internally Heated Pressure Vessel (IHPV) with an argon-hydrogen mixture pressure medium at the Institute of Mineralogy, Leibniz University of Hannover. The uncertainty in pressure and temperature was about ±5 MPa and ± 5 °C. The experiment was started at constant temperature for one day, and the temperature cycling technique (Erdmann and Koepke, 2016; Silva et al., 2017) was applied for 4 days (900 °C +/− 25 °C) in order to increase the sizes of the experimental phases, and left at constant temperature for 6 days. Oxygen fugacity (fO_2) was adjusted according to values of NNO (fO_2 imposed by the Nickel-Nickel Oxide buffer reaction) by adding the desired amount of hydrogen to the argon gas. Partial hydrogen pressure was monitored using a Shaw membrane during the run. The fO_2 was determined using the dissociation reaction of H_2O and the associated correlations between the H_2O dissociation constant (Pitzer and Sterner, 1995) and the standard state fugacity of H_2O (Robie et al.,

Table 1
Experiments performed and experimental conditions used.

Run	Starting rock	Exp. apparatus	T (°C)	t (days)	NaCl Fl[a] (wt%)	ϱ Fl[b] (g/cm³)	N. of runs[c]	Fl/R[d]	Newly-formed phases
IHB20-9	Ol gabbro cylinder	IHPV	900	10	20	0.55	1	0.07	Amp[f], melt, Pl, Ol, (Ilm), (Mag)
CSB50-1	Ol gabbro cylinder	CSPV	750	10	50	0.99	1	0.2	Amp, (Chl)[g], Pl, Cpx, (Ilm), (Mag)
CSB50-2	Ol gabbro cylinder	CSPV	750	10	50	0.99	2	0.2[e]	Amp, (Chl), Pl, Cpx, (Ilm), (Mag)
CSB20-1	Ol gabbro cylinder	CSPV	750	10	20	0.66	1	0.2	Amp, (Chl), Pl, Ol, (Ilm), (Mag)
CSB20-2	Ol gabbro cylinder	CSPV	750	10	20	0.66	2	0.2[e]	Amp, (Chl), Pl, Ol, Cpx, (Ilm), (Mag)
CSB6-1	Ol gabbro cylinder	CSPV	750	10	6	0.52	1	0.2	Amp, (Chl), Pl, Ol, (Ilm), (Mag)
CSBX50-1	Ol gabbro cylinder	CSPV	650	10	50	1.06	1	0.2	Amp, (Chl), Pl, Ol, Cpx, (Ilm), (Mag)
CSBX20-1	Ol gabbro cylinder	CSPV	650	10	20	0.74	1	0.2	Amp, (Chl), Pl, Ol, (Ilm), (Mag)
CSBX6-1	Ol gabbro cylinder	CSPV	650	10	6	0.60	1	0.2	Amp, (Chl), Pl, Ol, (Ilm), (Mag)
OB-600-C	Ol gabbro cylinder	CSPV	600	101	20	0.79	1	1	Amp, Chl, Pl, (Ilm), (Mag)
OB-500-C	Ol gabbro cylinder	CSPV	500	101	20	0.87	1	1	Amp, Chl, (Ilm), (Mag)

All experiments performed at pressures of 200 MPa and oxygen fugacity close to NNO. Number of runs indicates whether an experiment was run once (1), or whether solids were extracted after first run and run again adding a new batch of saline fluid (2).

[a] NaCl content of the starting fluid.

[b] Density of the corresponding pure NaCl-H_2O fluid at the experimental pressure and temperature conditions (calculated using equations of Driesner, 2007).

[c] N. (Number) of runs indicates whether an experiment was run once (1), or whether the solids of the first run were extracted and run again using a new batch of the same starting solution (2).

[d] Fl/R is the fluid-to-rock mass ratio.

[e] Solids run twice at Fl/R of 0.2 and hence approximately at Fl/R of ~0.4.

[f] Mineral abbreviations after Whitney and Evans (2010). Amp: amphibole; Pl: plagioclase; Ol: olivine; Ilm: ilmenite; Mag: magnetite; Chl: chlorite; cpx: clinopyroxene.

[g] Mineral name in brackets denotes small amounts (<~2 vol.%).

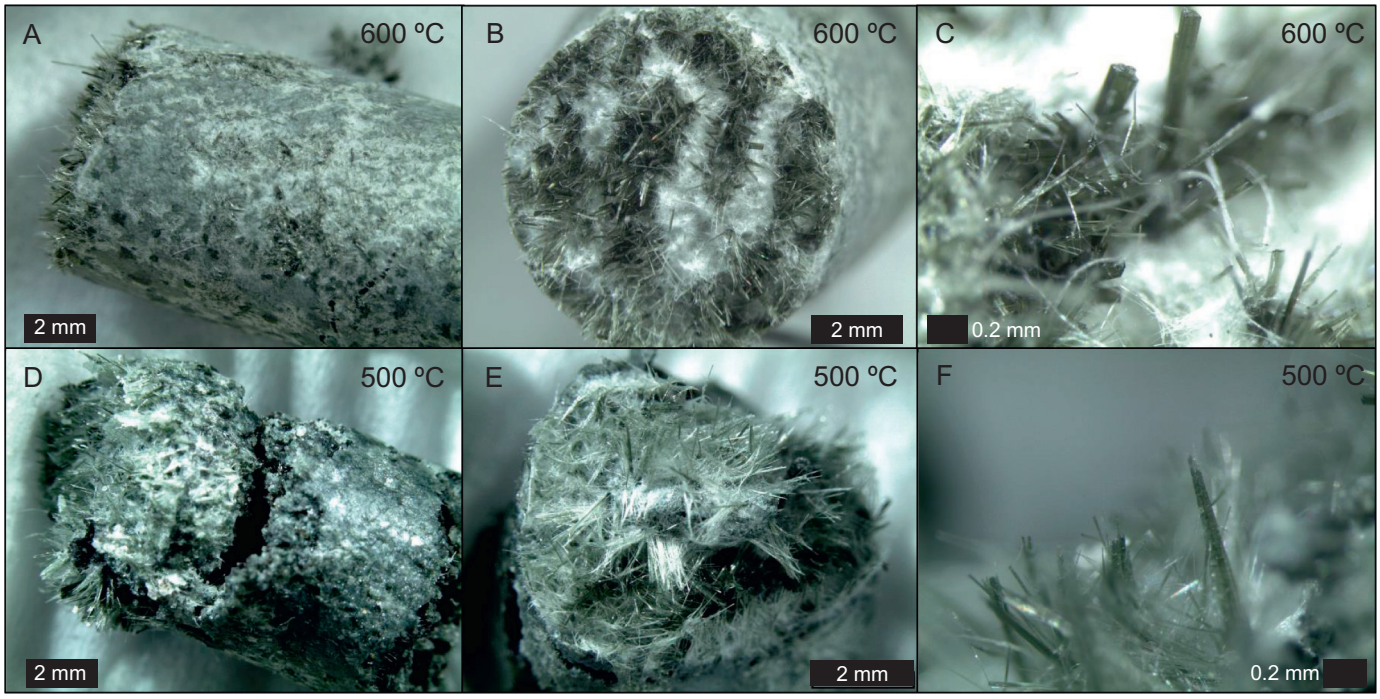

Fig. 4. Microscope images from experiments performed in CSPV at 600 °C and 500 °C (OB-600-C and OB-500-C) with a fluid/rock ratio of 1 and a duration of 101 days (image acquisition by Leica M205 C stereo microscope equipped with Leica DFC 295 camera system). Both experiments display prismatic and acicular amphibole crystals formed on the surface of the gabbro cylinder.

1978) and of H_2 (Shaw and Wones, 1964). The experiment was stopped by rapid quenching (~150 °C/s). Details on IHPV apparatus and applied techniques can be found in Berndt et al. (2002).

Subsolidus experiments were performed in two similar Cold Seal Pressure Vessel (CSPV) facilities, one at the Institute of Mineralogy in Hannover (750 and 650 °C), and the other at the Institute of Geosciences, Kiel University (600 and 500 °C), the latter with autoclaves constructed for large sample volumes. Calibrations were performed to check the heat distribution inside the furnace and autoclave and estimate the uncertainty in temperature and pressure of the experiments, which was ca. ±5 MPa and ± 5 °C for the runs at 650 to 750 °C and, given the larger temperature differences along the larger sample capsules, ± 7 °C at 500 and 600 °C. The oxygen fugacity in the hydrothermal environment of the vessel is imposed by the hydrogen fugacity along the water dissociation reaction in vicinity of the nickel-nickel oxide buffer (NNO) reaction from the Ni filler rods. However, due to the low permeability of the 0.2 mm thick gold capsules to hydrogen (Chou, 1986), attainment of redox equilibrium of the experimental systems with the autoclave atmosphere – particularly for the run at 500 °C – is not ensured (Allen and Seyfried, 2003). Experiments were terminated by removing the vessels from the furnace and subsequently cooling them using a compressed air flow for approximately 15 min close to room temperature.

Given the extent of suppression of the H_2O activity to be expected by the NaCl-rich fluids (Aranovich and Newton, 1996; Webster, 1992), the corresponding fO_2 (in bar) of the most NaCl-rich experiments (50 wt% NaCl or 0.24 X_{NaCl} solutions) should be lowered roughly by ~0.3 log units, but does not significantly affect fO_2 at lower NaCl concentrations.

Experimental capsules were examined for damage and weighed after each run to check for possible fluid leakage, in which case the contents of the capsule were discarded and the procedure was repeated again. When successful, the solid experimental products were extracted from the capsules, mounted on epoxy and polished for analysis. Excess fluid was not extracted. Microscope images of experimental products after extraction from capsules can be seen in Fig. 4.

2.3. Analytical techniques

Analysis of amphibole minerals from experimental charges have been conducted in-situ with electron probe microanalysis (EPMA) for major elements, minor Cl, and trace Cr, Ti, F. A Cameca SX100 electron microprobe equipped with 5 spectrometers and the software "Peak Sight" was used at the Institute of Mineralogy of the Leibniz University in Hannover, Germany. A 15 nA focussed beam current and a 15 kV acceleration voltage were used for analysis. The peak counting times of 10s were used for all elements (5 s background), except for Cl and F (30 s peak and 15 s background). For calibration of elemental measurements, the natural and synthetic standards used were albite (Na), wollastonite (Ca and Si), orthoclase (K), Durango apatite (P), Al_2O_3 (Al), Mn_2O_3 (Mn), TiO_2 (Ti), MgO (Mg), Fe_2O_3 (Fe), NaCl (Cl), and SrF_2 (F). To monitor analytical precision, each measurement was checked against the international amphibole standard Kakanui hornblende (USNM 143965) as reference material (Jarosewich et al., 1980). Representative analyses from amphibole EPMA measurements are given in Table 2. The amphibole formula calculation was done using a cation sum of 13 excluding Ca, Na, and K. Limits of detection (in wt%) in amphibole are: SiO_2: 0.04; TiO_2: 0.02; Al_2O_3: 0.04; FeO: 0.094, MnO: 0.06; MgO: 0.056; CaO: 0.06, NaO: 0.06; K: 0.014; Cr: 0.09; Cl: 0.003; F: 0.3.

3. Results

3.1. Suprasolidus experiments

The experiment run at 900 °C (IHB20-9) shows the presence of a melt phase (Fig. 5D). New amphibole crystallized in melt pools (about 10–20 μm grain size), in contact with plagioclase and olivine, sometimes as rims (5 μm grain size) around olivine, classified as magnesiohastingsite and tschermakite. Compositions of experimental amphibole

Table 2
EPMA analyses of newly-formed amphibole from experimental products (representative analyses) and starting amphibole (average).

				wt%													T position[e]		C position								B position			A position		W position		
Run	Temp. (°C)	Amph. Name[a]	high Cl[b]	SiO_2	TiO_2	Al_2O_3	Cr_2O_3	MnO[c]	FeO[d]	MgO	CaO	Na_2O	K_2O	Cl	O-Cl	Total	Si	Al	Ti	Al	Cr	Fe^{3+}	Mn^{2+}	Fe^{2+}	Mg	Mn^{3+}	Mg	Ca	Na	Na	K	Cl	OH	Mg#
IHB20-9	900	Ts		43.28	0.40	11.68	0.00	0.17	11.77	15.24	10.59	3.02	0.03	0.13	−0.03	96.28	6.25	1.75	0.04	0.24		1.31	0.02	0.12	3.28	0.00	0.00	1.64	0.36	0.48	0.01	0.031	1.97	96.6
IHB20–9	900	Mhs		42.80	0.84	14.11	0.00	0.18	10.08	16.00	10.70	3.39	0.03	0.06	−0.01	98.18	6.03	1.97	0.09	0.37		1.19	0.00	0.00	3.33	0.02	0.03	1.62	0.36	0.57	0.01	0.013	1.99	100.0
IHB20-9	900	Ts	x	42.60	2.12	11.56	0.00	0.21	14.10	14.29	10.13	3.22	0.01	0.48	−0.11	98.61	6.08	1.92	0.23	0.02		1.45	0.03	0.23	3.04	0.00	0.00	1.55	0.45	0.44	0.00	0.117	1.88	92.9
CSB50-1	750	Mhs		42.91	0.19	11.71	0.00	0.10	13.20	15.63	10.66	3.98	0.02	0.07	−0.02	98.45	6.11	1.89	0.02	0.08		1.42	0.01	0.15	3.32		0.00	1.63	0.37	0.72	0.00	0.016	1.98	95.6
CSB50-1	750	Ed		45.67	0.92	8.79	0.05	0.10	10.02	16.44	10.33	4.04	0.00	0.04	−0.01	96.40	6.62	1.38	0.10	0.12	0.01	0.72	0.01	0.50	3.55		0.00	1.60	0.40	0.74	0.00	0.010	1.99	87.7
CSB50-1	750	Mhs	x	43.89	0.22	10.39	0.00	0.14	12.40	14.93	10.63	3.51	0.00	0.26	−0.06	96.30	6.41	1.59	0.03	0.20		1.03	0.02	0.49	3.25		0.00	1.66	0.34	0.66	0.00	0.063	1.94	87.0
CSB50-2	750	Mhs		43.00	1.08	11.84	0.22	0.15	11.78	15.10	10.62	3.68	0.01	0.06	−0.01	97.55	6.18	1.82	0.12	0.19	0.03	1.07	0.02	0.34	3.24		0.00	1.64	0.37	0.66	0.00	0.016	1.98	90.4
CSB50-2	750	Ed		45.74	0.92	8.96	0.10	0.05	11.67	15.99	10.37	4.01	0.00	0.07	−0.01	97.88	6.56	1.45	0.10	0.07	0.01	0.87	0.01	0.53	3.42		0.00	1.59	0.41	0.71	0.00	0.016	1.98	86.5
CSB50-2	750	Mhs	x	44.58	1.31	9.65	0.01	0.22	11.53	15.24	10.48	3.71	0.00	0.34	−0.08	97.00	6.48	1.52	0.14	0.13	0.00	0.80	0.03	0.60	3.30		0.00	1.63	0.37	0.68	0.00	0.085	1.92	84.6
CSB20-1	750	Mhs		42.67	0.81	12.63	0.03	0.25	11.16	14.46	10.56	3.62	0.01	0.11	−0.03	96.29	6.21	1.79	0.09	0.38	0.00	0.91	0.03	0.45	3.14		0.00	1.65	0.35	0.67	0.00	0.028	1.97	87.4
CSB20-1	750	Mhb		46.17	0.69	9.00	0.00	0.15	10.58	16.49	10.21	3.17	0.00	0.08	−0.02	96.53	6.61	1.39	0.08	0.13	0.00	1.11	0.02	0.16	3.52		0.00	1.57	0.44	0.45	0.00	0.020	1.98	95.8
CSB20-1	750	Ts		44.41	0.43	10.57	0.00	0.22	11.08	16.47	10.20	3.24	0.01	0.13	−0.03	96.71	6.35	1.65	0.05	0.13	0.00	1.32	0.00	0.00	3.48	0.03	0.03	1.56	0.41	0.49	0.00	0.03	1.97	100.0
CSB20-1	750	Ts	x	44.41	0.43	10.57	0.00	0.22	11.08	16.47	10.20	3.24	0.01	0.13	−0.03	96.71	6.35	1.65	0.05	0.13	0.00	1.32	0.00	0.00	3.48	0.03	0.03	1.56	0.41	0.49	0.00	0.031	1.97	100.0
CSB20-2	750	Mhs		43.77	0.48	11.36	0.00	0.23	11.81	15.05	9.95	3.68	0.00	0.07	−0.02	96.39	6.32	1.68	0.05	0.25		1.21	0.03	0.22	3.24		0.00	1.54	0.46	0.57	0.00	0.018	1.98	93.7
CSB20-2	750	Mhb		51.18	0.09	4.99	0.00	0.24	8.63	18.40	10.98	1.90	0.01	0.12	−0.03	96.51	7.23	0.77	0.01	0.07		0.83	0.03	0.19	3.88		0.00	1.66	0.34	0.18	0.00	0.028	1.97	95.4
CSB20-2	750	Ed		45.46	0.94	9.65	0.00	0.28	11.65	15.08	9.98	3.48	0.00	0.08	−0.02	96.58	6.57	1.43	0.10	0.21		0.96	0.04	0.45	3.25		0.00	1.54	0.46	0.52	0.00	0.019	1.98	87.8
CSB20-2	750	Mhs	x	43.47	2.10	10.69	0.09	0.20	12.80	13.54	10.77	3.47	0.01	0.35	−0.08	97.40	6.37	1.63	0.23	0.21	0.01	0.59	0.02	0.98	2.96		0.00	1.69	0.31	0.67	0.00	0.088	1.91	75.1
CSB6-1	750	Mhs		38.48	0.47	15.73	0.00	0.21	17.54	9.41	12.11	3.24	0.04	0.02	0.00	97.25	5.80	2.20	0.05	0.59		0.63	0.03	1.58	2.12		0.00	1.96	0.04	0.90	0.01	0.005	2.00	57.3
CSB6-1	750	Ts		43.50	0.02	11.55	0.00	0.14	14.19	14.54	10.25	3.30	0.03	0.06	−0.01	97.57	6.23	1.77	0.00	0.18		1.52	0.02	0.18	3.10		0.00	1.57	0.43	0.49	0.01	0.015	1.99	94.5
CSB6-1	750	Mhb		45.85	0.26	9.02	0.00	0.19	12.98	15.21	10.17	2.60	0.01	0.07	−0.01	96.36	6.60	1.41	0.03	0.13		1.36	0.02	0.20	3.26		0.00	1.57	0.43	0.29	0.00	0.016	1.98	94.2
CSB6-1	750	Mhb	x	50.61	0.08	6.21	0.00	0.15	9.77	18.52	9.94	1.39	0.16	0.13	−0.03	96.93	7.08	0.92	0.01	0.10		1.14		0.00	3.73	0.02	0.13	1.49	0.38	0.00	0.03	0.030	1.97	100.0
CSBX50-1	650	Mhs		42.64	1.55	10.95	0.00	0.14	13.67	13.23	10.73	3.24	0.01	0.07	−0.02	96.22	6.30	1.70	0.17	0.21		0.82	0.02	0.87	2.91		0.00	1.70	0.30	0.63	0.00	0.019	1.98	77.0
CSBX50-1	650	Mhb		44.10	0.51	9.88	0.00	0.16	18.94	10.57	10.82	2.48	0.00	0.15	−0.03	97.57	6.53	1.48	0.06	0.25		0.98	0.02	1.37	2.33		0.00	1.72	0.29	0.43	0.00	0.037	1.96	63.0
CSBX50-1	650	Ts		45.49	0.06	11.34	0.00	0.22	11.34	16.13	10.99	2.79	0.03	0.08	−0.02	98.45	6.39	1.62	0.01	0.26		1.27	0.03	0.06	3.37		0.00	1.65	0.35	0.41	0.01	0.019	1.98	98.1
CSBX50-1	650	Ts	x	45.75	0.68	9.82	0.00	0.19	13.20	15.01	9.48	2.95	0.00	0.46	−0.10	97.44	6.51	1.50	0.07	0.15		1.50	0.02	0.07	3.18		0.00	1.44	0.56	0.26	0.00	0.110	1.89	97.7
CSBX20-1	650	Ts		44.26	1.36	10.74	0.07	0.26	12.76	14.03	10.97	2.64	0.00	0.06	−0.01	97.14	6.41	1.59	0.15	0.24	0.01	0.90	0.03	0.64	3.03		0.00	1.70	0.30	0.44	0.00	0.015	1.99	82.5
CSBX20-1	650	Mhs		42.58	0.45	11.17	0.00	0.33	15.36	13.02	10.78	2.99	0.00	0.04	−0.01	96.71	6.25	1.75	0.05	0.18		1.24	0.04	0.65	2.85		0.00	1.69	0.31	0.54	0.00	0.010	1.99	81.5
CSBX20-1	650	Mhb		47.27	0.41	6.99	0.01	0.29	14.14	14.52	10.91	2.01	0.01	0.07	−0.02	96.60	6.86	1.14	0.05	0.06	0.00	1.02	0.04	0.69	3.14		0.00	1.70	0.30	0.26	0.00	0.017	1.98	81.9
CSBX20-1	650	Mhs	x	41.95	0.05	11.03	0.00	0.18	17.28	12.52	10.70	3.16	0.02	0.10	−0.02	96.99	6.18	1.82	0.01	0.09		1.43	0.02	0.70	2.75		0.00	1.69	0.31	0.59	0.00	0.026	1.97	79.8
CSBX6-1	650	Mhb		46.93	0.22	9.14	0.00	0.36	13.11	15.06	10.50	1.54	0.02	0.04	−0.01	96.91	6.66	1.34	0.02	0.19		1.48	0.04	0.07	3.19		0.00	1.60	0.40	0.02	0.00	0.009	1.99	97.7
CSBX6-1	650	Ts		44.07	0.51	11.44	0.00	0.25	13.17	14.64	10.53	2.16	0.01	0.05	−0.01	96.82	6.30	1.70	0.06	0.22		1.55	0.03	0.03	3.12		0.00	1.61	0.39	0.21	0.00	0.012	1.99	99.2
CSBX6-1	650	Mhs		41.13	0.27	13.67	0.03	0.17	14.46	12.83	12.03	2.83	0.01	0.04	−0.01	97.45	6.02	1.98	0.03	0.38		0.97	0.02	0.81	2.80		0.00	1.89	0.11	0.69	0.00	0.010	1.99	77.7
CSBX6-1	650	Ts	x	42.84	0.17	12.71	0.05	0.26	16.26	12.03	10.58	2.20	0.01	0.07	−0.02	97.17	6.21	1.80	0.02	0.38	0.01	1.48	0.03	0.50	2.60		0.00	1.64	0.36	0.26	0.00	0.018	1.98	84.0
OB-600-C	600	Mhs		40.81	1.02	12.31	0.03	0.18	17.30	10.82	11.12	2.97	0.01	0.03	−0.01	96.60	6.11	1.89	0.12	0.28	0.00	0.95	0.02	1.22	2.41		0.00	1.78	0.22	0.65	0.00	0.009	1.99	66.5
OB-600-C	600	Hs		39.76	0.29	13.98	0.10	0.15	21.77	7.87	11.16	3.30	0.00	0.03	−0.01	98.40	5.97	2.03	0.03	0.44	0.01	0.96	0.02	1.77	1.76		0.00	1.80	0.20	0.76	0.00	0.007	1.99	49.8
OB-600-C	600	Fprg		39.34	1.82	17.42	0.10	0.03	19.03	7.11	11.04	3.59	0.05	0.02	−0.01	99.53	5.82	2.18	0.20	0.86	0.01	0.36	0.00	1.99	1.57		0.00	1.75	0.25	0.78	0.01	0.006	1.99	44.0
OB-600-C	600	Mhb		53.07	0.77	3.57	0.10	0.06	7.35	19.20	12.63	0.90	0.06	0.06	−0.01	97.76	7.44	0.56	0.08	0.03	0.01	0.31	0.01	0.55	4.01		0.00	1.90	0.10	0.14	0.01	0.014	1.99	87.9
OB-600-C	600	Mhs	x	38.70	1.99	16.00	0.10	0.09	16.91	10.31	9.95	3.89	0.07	0.24	−0.05	98.21	5.67	2.33	0.22	0.43	0.01	1.20	0.01	0.87	2.25		0.00	1.56	0.44	0.67	0.01	0.060	1.94	72.2
OB-500-C	500	Mhs		43.48	0.74	12.90	0.10	0.17	16.87	10.82	11.03	2.94	0.00	0.03	−0.01	99.07	6.30	1.70	0.08	0.51	0.01	0.77	0.02	1.27	2.34		0.00	1.71	0.29	0.54	0.00	0.008	1.99	64.7
OB-500-C	500	Hs		40.78	0.07	11.62	0.10	0.21	24.71	5.88	11.53	2.13	0.01	0.15	−0.03	97.15	6.30	1.71	0.01	0.41	0.01	0.81	0.03	2.38	1.35		0.00	1.91	0.09	0.54	0.00	0.038	1.96	36.3
OB-500-C	500	Ts		43.00	0.35	12.54	0.10	0.13	16.85	10.69	11.18	2.51	0.02	0.03	−0.01	97.38	6.33	1.67	0.04	0.51	0.01	0.82	0.02	1.26	2.35		0.00	1.76	0.24	0.48	0.00	0.006	1.99	65.1
OB-500-C	500	Mhb		46.93	0.38	8.54	0.10	0.26	13.16	14.78	11.22	1.95	0.01	0.09	−0.02	97.39	6.73	1.27	0.04	0.18	0.01	1.00	0.03	0.58	3.16		0.00	1.73	0.28	0.27	0.00	0.022	1.98	84.6
OB-500-C	500	Mhb	x	52.50	0.11	3.57	0.10	0.17	9.44	18.28	11.88	0.94	0.02	0.20	−0.05	97.17	7.41	0.59	0.01	0.00	0.01	0.72	0.02	0.40	3.85		0.00	1.80	0.20	0.05	0.00	0.049	1.95	90.6
Starting amphibole[f]		Mhs		42.35	3.59	11.39	0.42	0.16	9.74	15.61	11.35	3.16	0.20	0.00	0.00	97.97	6.09	1.91	0.39	0.02	0.05	0.64	0.02	0.53	3.35		0.00	1.75	0.25	0.63	0.04	0.000	2.00	86.4
			1 σ	0.63	0.32	0.40	0.06	0.06	0.43	0.43	0.21	0.17	0.02	0.00																				

Fluorine always below limit of detection; values for the structual formula are atoms per formula unit (a.p.f.u.), calculated using a sum of 13 cations excluding Ca, Na, K.

[a] According to the mineral abbreviations by Whitney and Evans (2010). Ed: Edenite; Fprg: ferro-pargasite; Hst: hastingsite; Mhb: magnesio-hornblende; Mhs: magnesio-hastingsite; Ts: tschermakite.

[b] Amphibole strongly enriched in chlorine.

[c] FeO = FeO^{total}; MnO = MnO^{total}.

[d] FeO = FeO^{total}; MnO = MnO^{total}.

[e] Amphibole structural sites according to Locock (2014).

[f] Average of amphibole analyses of the starting material; number of analyses = 8; one standard deviation is shown; starting material: olivine gabbro drilled during IODP Leg 153, sample: 153- 920B-13R-4, 32–36 cm.

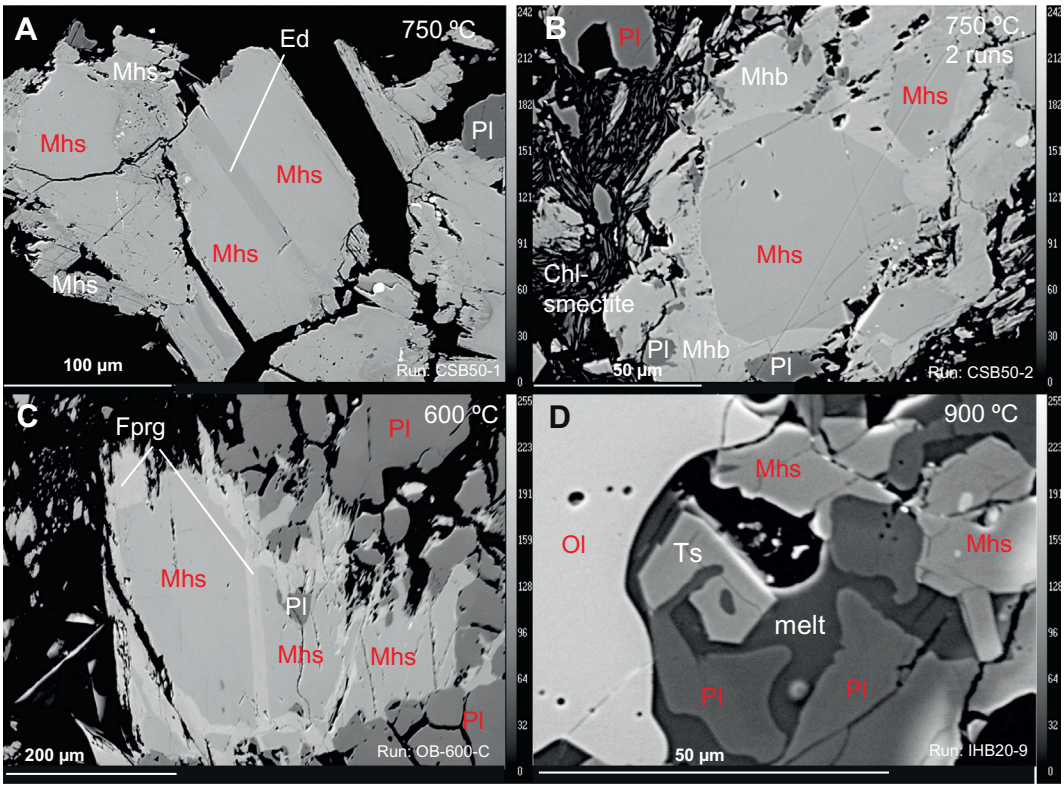

Fig. 5. BSE images of experimental products. Pre-existing minerals (e.g. starting amphibole) indicated in red. A: Experiment at 750 °C, with 50 wt% NaCl fluid. Product amphibole (magnesio-hastingsite and edenite) forms coherent domains on the rim of the starting amphibole. B: Experiment at 750 °C, with 50 wt% NaCl fluid, run twice with an added batch of NaCl-rich fluid. Relatively large crystals of starting amphibole are replaced by porous domains of magnesio-hornblende with plagioclase inclusions. Aggregates of chlorite/smectite mixed layer minerals are visible in the matrix. C: Experiment performed at 600 °C, with 20 wt% NaCl fluid. Note the overgrowth of product ferro-pargasite (rim) replacing the starting amphibole (core). D: Experiment at 900 °C, with 20 wt% NaCl in fluid, showing newly formed tschermakite amphibole and small melt pools, as well as relict plagioclase, olivine, and starting amphibole. Mineral abbreviations after Whitney and Evans (2010); Ed: Edenite; Fprg: ferro-pargasite; Hst: hastingsite; Mhb: magnesio-hornblende; Mhs: magnesio-hastingsite; Ts: tschermakite; Pl: plagioclase; Ol: olivine.

plotted in Figs. 6A and 7A show little departure from the composition of the starting amphibole, except for variations in Mg and slightly lower ^{IV}Al. TiO_2 contents of newly-crystallized amphibole show variations between 0.5 wt% and ~ 2 wt%, depending on local availability of Ti (i.e., local presence of a Fe—Ti oxide phase). Cl contents in product amphibole are mostly above 0.15, reaching maximum Cl contents of 0.48 wt%. The coexisting melt phase is evolved and enriched in SiO_2, similar to felsic melts produced by hydrous partial melting of oceanic gabbros (Koepke et al., 2004; 2007), and rich in Cl (0.6 to 0.9 wt%). Excess fluid was not detected after the experimental run.

3.2. Subsolidus experiments

After experiments, relics of the initial olivine gabbro assemblage were preserved in all runs. In general, a decrease in the amount of primary olivine, clinopyroxene, and magnetite in the starting gabbro can be observed, especially in multiple-run experiments, with a relative increase in plagioclase and amphibole in newly-formed phases. Product amphibole occurs as rims around cores of the starting amphibole (Fig. 5), and crystallizing along grain boundaries, in cracks, and as outward-growing prismatic crystals (Fig. 4). Secondary plagioclase, olivine, and clinopyroxene have been identified together with the newly-formed amphibole. Interstitial growth of chlorite-smectite was observed, especially in lower temperature runs (Fig. 5).

3.2.1. Experimental runs at 750 °C

Product amphibole crystals measured in experiments run at 750 °C are classified as magnesio-hastingsite, magnesio-hornblende, tschermakite and edenite (Leake et al., 1997), ranging from significantly higher Si (>7 atoms per formula unit (a.p.f.u.)) to lower Si (~5.2 a.p.f.u.) than the starting amphibole (Fig. 6B). TiO_2 contents are below 1.5 wt%, and Mg# ($100 * Mg/(Mg + Fe^{2+})$) ranges from 57 to 100. A-site occupancy (mainly Na), is variable, from 0.2 to 0.9 a.p.f.u. (Table 2).

The effects of salinity are reflected in the Na content and A-site occupancy of newly-formed amphibole (Fig. 6B). Higher NaCl concentration in the experimental fluid resulted in higher Na contents in product amphibole formed during experiments with 50 wt% NaCl (0.9–1.15 total Na a.p.f.u.) in relation to experiments run with a fluid with 20 wt% NaCl (0.5–1 total Na a.p.f.u.). Likewise, experiments with 20 wt% NaCl have higher Na contents than experiments performed with a 6 wt% NaCl fluid (0.38–0.95 total Na a.p.f.u.). In addition, in terms of Cl content, experiments performed with 50 wt% NaCl fluid result in higher maximum Cl contents (0.26 wt% Cl) than experiments performed with 20 wt% NaCl (0.13 wt% Cl), however, this difference is not observed in experiments run a second time. Experiments run with 6 wt% Cl in fluid also reach a maximum of 0.13 wt% Cl (Fig. 7B).

Experiments run a second time (CSB50-2, CSB20-2) result in higher Cl contents (0.34 and 0.35 wt% Cl, respectively) than experiments of the same characteristics run a single time (0.26 wt% Cl for CSB50–1, and 0.13 wt% Cl for CSB20-1).

3.2.2. Experimental runs at 650 °C

Experimental products measured after runs at 650 °C correspond to magnesio-hastingsite, magnesio-hornblende, tschermakite and edenite (Leake et al., 1997), with Si ranging between 6 and 6.9 a.p.f.u. (Fig. 6C). TiO_2 contents are below 1.6 wt%, and Mg# is between 63 and 98. A-site occupancy in newly-formed amphibole is generally below that of the starting amphibole (0.63 a.p.f.u.).

Effect of fluid salinity is reflected in significantly higher maximum Cl contents (0.47 wt%) measured in amphibole formed in experiments run

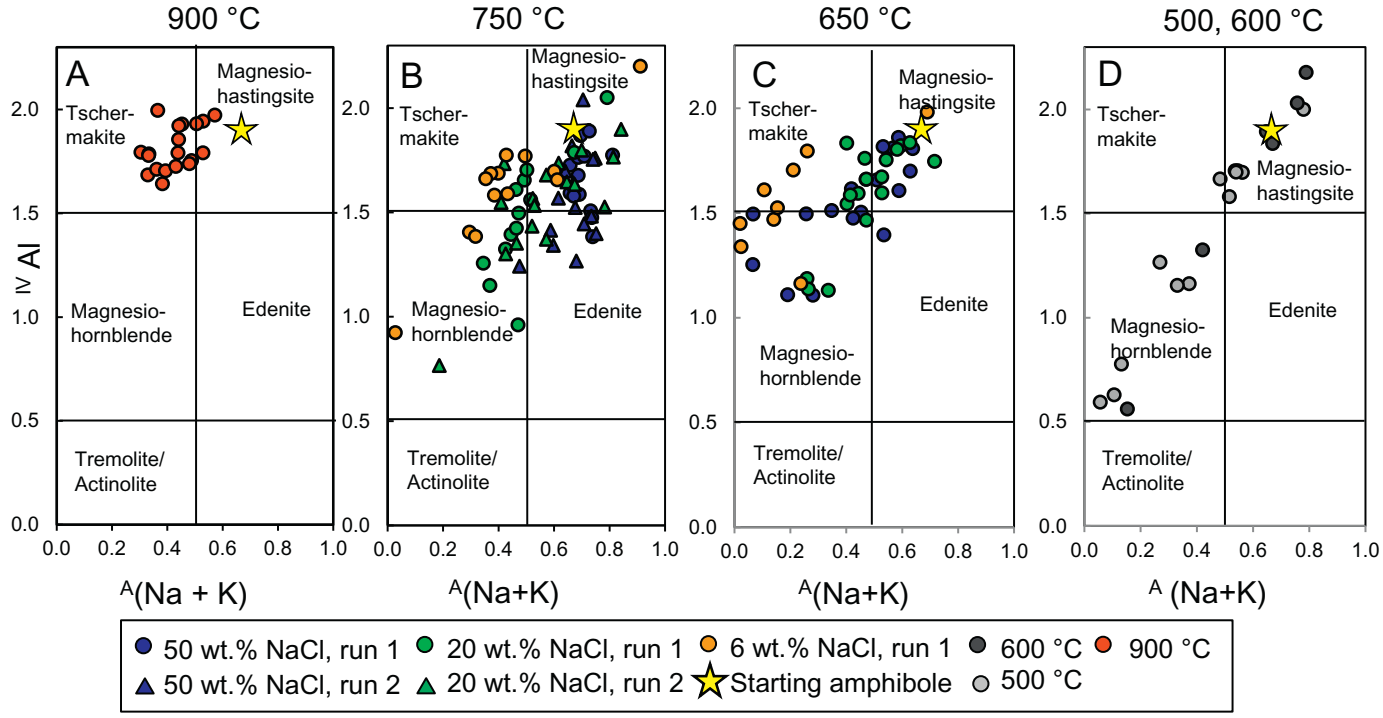

Fig. 6. Diagrams showing ^{IV}Al vs. ^{A}(Na + K) of product amphibole formed during experiments. Formula calculated using a sum of 13 cations excluding Ca, Na and K. Fields and classification after Leake et al. (1997). Stars denote starting amphibole composition (magnesio-hastingsite). A corresponds to experiment IHB20-9; B to experiments CSB50-1, CSB50-2, CSB20-1, CSB20-2, CSB6-1; C to experiments CSBX50-1, CSBX20-1, CSBX6-1; and D to experiments OB-600-C and OB-500-C.

with a 50 wt% NaCl fluid, vs. Cl contents of 0.10 and 0.07 wt% in amphibole from experiments run at 650 °C with a 20 wt% and a 6 wt% starting solution, respectively (Fig. 7C). Additionally, total Na and A-site occupancy are lowest in experiments run with a concentration of 6 wt% NaCl in fluid (total Na: 0.4–0.8).

3.2.3. Experimental runs at 600 and 500 °C

In experiments run at 600 and 500 °C at a water/rock ratio of 1, the growth of new amphibole can be observed together with secondary plagioclase (Fig. 5C). As evident in Fig. 4, acicular and prismatic amphibole phases are found crystallizing on the surface of the gabbro cylinder and interstitially. Interstitially, we find a matrix of chlorite – smectite mixed layers (accurate analysis with EPMA was not possible due to small grain size). Experimental products of the 500 °C run show a higher proportion of hydrous minerals and a greater extent of replacement of the original assemblage than the products of the run at 600 °C.

Measured amphibole product phases are classified as hastingsite, magnesio-hastingsite, magnesio-hornblende, ferro-pargasite, and tschermakite (Leake et al., 1997). These products show a wide range of Si contents, from <6 to 7.5 a.p.f.u., TiO_2 contents below 2 wt%, and Mg# between 36 and 91. A-site occupancy ranges from 0 to 0.8 a.p.f.u (Fig. 6D).

Maximum Cl contents obtained at 600 °C are measured in magnesio-hastingsite (0.24 wt% Cl) and in Si-rich magnesio-hornblende at 500 °C (0.20 wt% Cl) (Fig. 7D).

4. Discussion

4.1. Compositional variations of newly-formed amphibole

In terms of metamorphic facies, the chosen experimental temperatures correspond to a variation from granulite facies (900 °C), via upper amphibolite facies (750 °C), lower amphibolite facies (650 and 600 °C) down to greenschist facies (500 °C). Although experiments were conducted under a given temperature, amphibole compositions do not cluster in one specific field, but show a large variation from magnesio-hastingsite, through tschermakite or edenite, to magnesio-hornblende with high Si (~7.5, close to actinolitic compositions) (Fig. 6). We find that Si contents in product amphibole increase with decreasing temperature (e.g., Gillis et al., 2003). The presence of amphibole in settings of high temperature hydrothermal alteration with varying Si and Cl contents is not uncommon and is mostly associated with hydrothermal fluids that have cooled significantly, down to approximately 500 °C and below (Enami et al., 1999; Ito and Anderson, 1983; Silantyev et al., 2008). Only in the suprasolidus run (900 °C), product amphibole phases cluster in a relatively small area in comparison to the other runs under subsolidus conditions – between the tschermakite and magnesio-hastingsite fields. Such high-Al amphibole phases typically form under high temperatures (Gillis et al., 2003). In 750 °C runs, at the transition between granulite and upper amphibolite facies, some of the amphibole products show magnesio-hornblende compositions that are relatively low in ^{A}(Na + K) and ^{IV}Al in the tetrahedral site, consistent with their hydrothermal origin (Gillis et al., 2003).

4.2. Cl incorporation in amphibole

The incorporation of Cl – a large anion in comparison to OH and F – involves the deformation of part of the amphibole crystal structure, constraining cation incorporation into the mineral (Makino and Tomita, 1993; Oberti et al., 1993; Volfinger et al., 1985). This involves preferentially incorporating larger cations like Fe^{2+} instead of Mg (leading to Mg—Cl avoidance), ^{IV}Al instead of Si, and K instead of Na when accommodating Cl into the OH site (Aranovich and Safonov, 2018; Kullerud, 1996; Léger et al., 1996; McCormick and McDonald, 1999 and references therein). However, such correlations between cations, and between cations and anions, are mainly observed in amphiboles formed in Cl-saturated environments. In our experimental results, there is a lack of correlation between amount of Cl incorporated in amphibole and Fe^{2+}, Mg, K, Na and ^{IV}Al contents. This result exemplifies the fact that at low levels of Cl incorporation in amphibole (in this

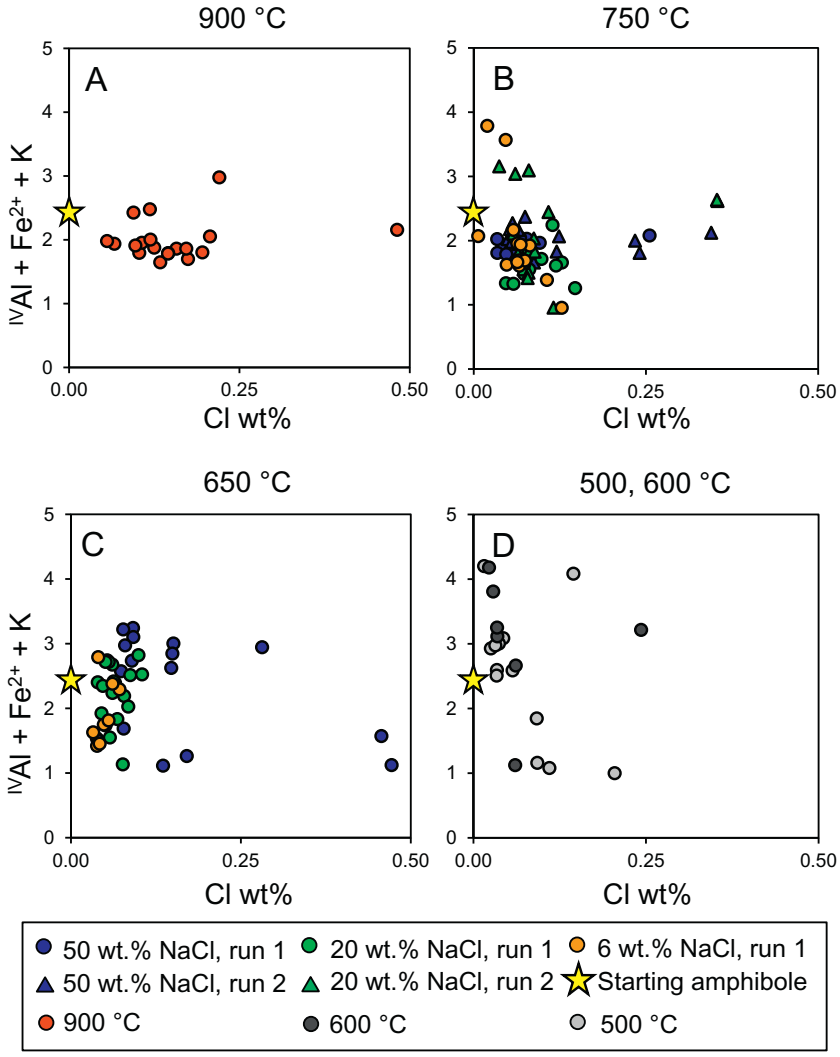

Fig. 7. Diagrams showing the relationships between ^{IV}Al + Fe^{2+} + K vs. Cl wt% measured in amphibole products. Formula calculated using a sum of 13 cations excluding Ca, Na and K. Fields and classification after Leake et al. (1997). Stars denote starting amphibole composition (magnesio-hastingsite). A corresponds to experiment IHB20-9; B to experiments CSB50-1, CSB50-2, CSB20-1, CSB20-2, CSB6-1; C to experiments CSBX50-1, CSBX20-1, CSBX6-1; and D to experiments OB-600-C and OB-500-C.

case, up to 0.5 wt% Cl), the abovementioned compositional correlations may not be relevant (Oberti et al., 1993). Chan et al. (2016, Fig. 2) reported a direct correlation between increasing fluid salinity and increasing Cl in amphibole up to about 0.2 wt% (0.05 a.p.f.u.). Above this threshold, at increasing fluid salinities, the increase of Cl in amphibole slows down until the fluid has passed Cl saturation (Chan et al., 2016). Since only mildly Cl-rich amphibole was formed during our experiments, it is possible that excess fluid remaining after each run remained Cl-rich, however, without adequate analysis of the fluid and mass balance calculations it is difficult to assume the composition of excess fluids.

4.3. Application to nature

When comparing our experimental results to amphibole occurrences in nature (Fig. 2 – previous work) we observe that products are similar to magnesio-hornblende with Cl < 0.4 wt% Cl. In this case, the fluid reacting with the host rock is below NaCl saturation, such as the fluid used in our experiments. The amphibole labelled as high-Ti pargasite is comparable to the amphibole formed in experiment IHB20-9, at suprasolidus conditions, and the amphibole labelled as magnesio-hornblende is analogous to some of the products of experiments at 650 and 750 °C.

Our experimental amphibole products from all runs clearly overlap with amphibole compositions measured in natural rocks from the oceanic crust in different settings (fast- and slow-spreading systems) drilled at the ocean floor and ophiolites (Alt et al., 2010; Bosch et al., 2004; Coogan et al., 2001; Gillis et al., 2003; Ito and Anderson, 1983; Koepke et al., 2008, 2011; Silantyev et al., 2008; Vanko, 1986 and Wolff, 2014) (Fig. 8).

In terms of Cl incorporation in amphibole, data from studies that measured relatively high Cl contents (>0.3 a.p.f.u. Cl) (Kullerud, 1996; Silantyev et al., 2008; Vanko, 1986; Wolff, 2014) show a correlation between ^{IV}Al and increasing Cl content (Fig. 8B). Conversely, all studies of natural samples shown in Fig. 8 (and the present experimental study) also measured amphibole with far lower Cl contents, including chlorine-free hydrothermal amphibole. This variability in Cl content is probably due to local changes in Cl activity in the fluid.

4.4. Comparison to other experimental studies

The Cl contents obtained in amphibole from all our experiments have been plotted against the NaCl content of the fluid used in each experiment (Fig. 9A) and against experimental temperature (Fig. 9B), in order to assess the influence of these two variables on Cl incorporation in amphibole. Results from other experimental studies were plotted alongside ours for comparison (Chan et al., 2016; Khodorevskaya and

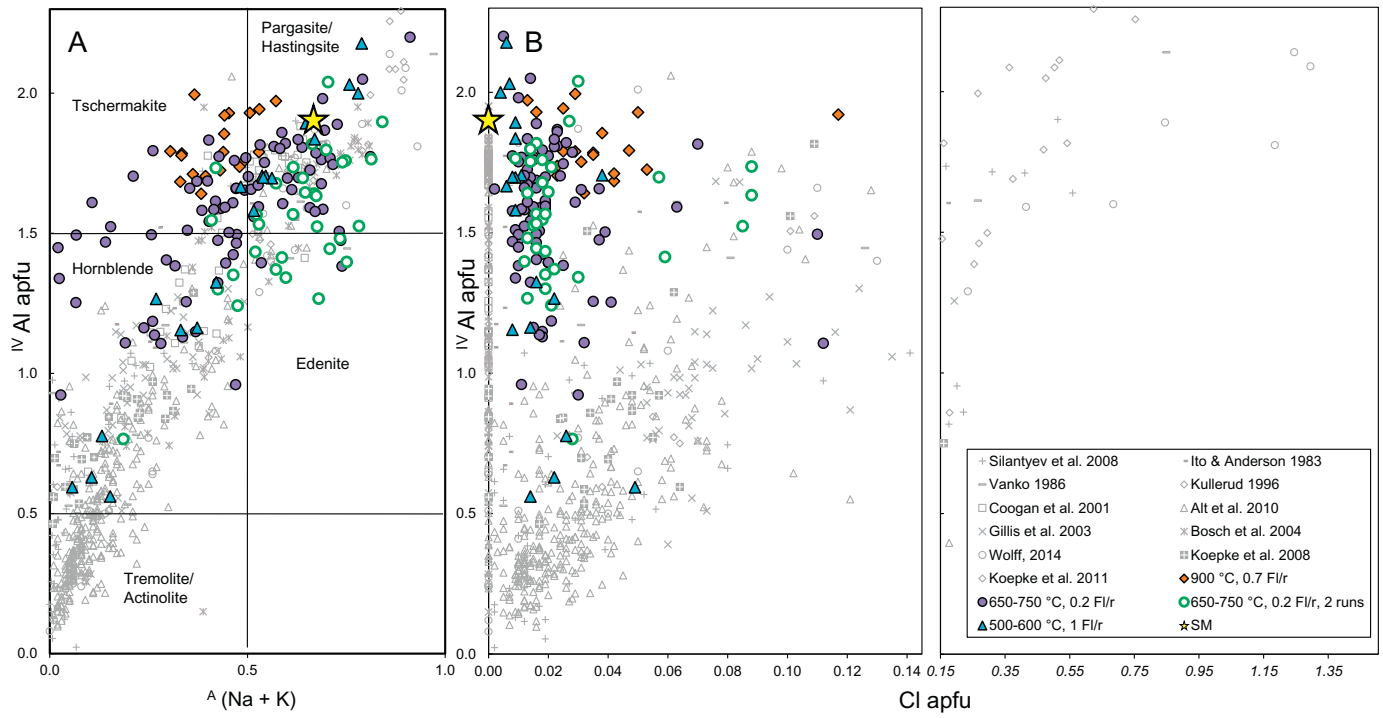

Fig. 8. A: Diagram showing ^{IV}Al vs. ^{A}(Na + K) of experimentally-formed amphibole. Names of fields after Leake et al. (1997), hornblende field includes magnesio-hornblende and ferro-hornblende, tschermakite field includes tschermakite and ferro-tschermakite, pargasite/hastingsite field includes magnesio-hastingsite and ferro-pargasite. B: ^{IV}Al vs. Cl a.p.f.u. (atoms per formula unit). Amphibole formed at suprasolidus conditions (900 °C) and low water/rock ratios (0.07) is denoted by diamonds (incipient hydrothermal activity), amphibole formed at high temperature subsolidus conditions (650 to 750 °C) and at a fluid/rock ratio of 0.2 is denoted by circles (full circles: experiments run once; open circles: experiments run a second time with a new batch of fluid), and amphibole formed at intermediate temperature subsolidus conditions (500 to 600 °C) with a higher fluid/rock ratio (1) is denoted by triangles. Our experimental data has been contrasted with amphibole analyses from various studies of amphibole hosted in natural oceanic gabbro affected by hydrothermal activity and that investigate the transition from the suprasolidus to the subsolidus regime (Alt et al., 2010; Coogan et al., 2001; Gillis et al., 2003; Koepke et al., 2008; Koepke et al., 2011; Kullerud, 1996; Silantyev et al., 2008; Vanko, 1986). Note that two different scales were used for the horizontal axis in B to display the wide range of Cl concentrations in the natural amphiboles.

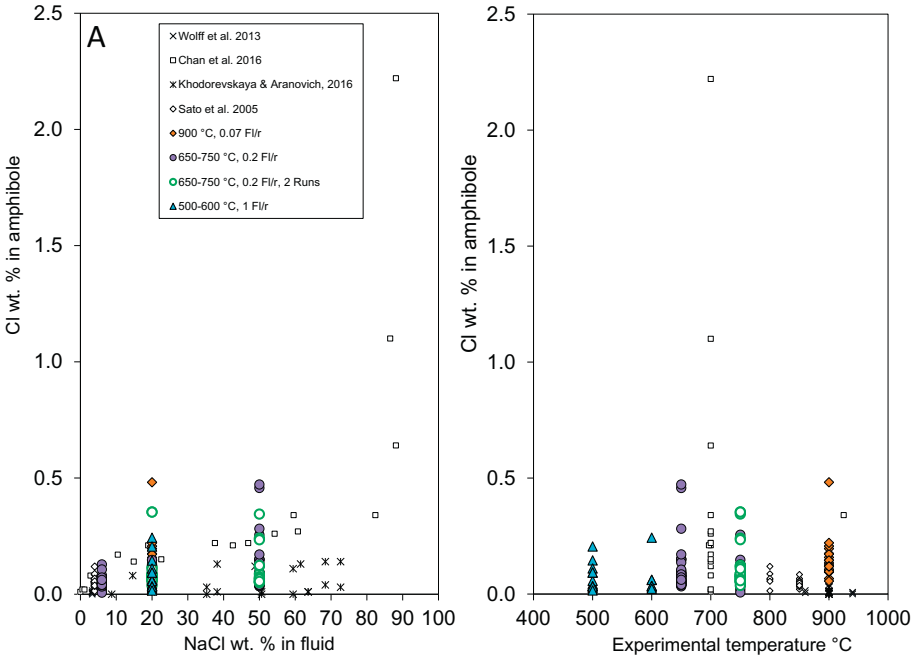

Fig. 9. Cl concentration in experimental amphibole versus experimental parameters. A: Cl wt% of newly formed amphibole for each experiment, plotted against NaCl wt% in aqueous fluid used in the experiment. B: Cl wt% in experimental amphibole for each experiment, plotted against experimental temperature. Data from previous experimental studies has been plotted against our experimental results for comparison: Sato et al. (2005), Wolff et al. (2013), Chan et al. (2016), Khodorevskaya and Aranovich (2016).

Aranovich, 2016; Sato et al., 2005; Wolff et al., 2013), all showing consistent trends of amphibole Cl with fluid Cl contents alongside the observations of Chan et al. (2016).

Chan et al. (2016) found that increasing the concentration of NaCl in the fluid would influence Cl incorporation in the amphibole up to about $X_{NaCl} = 0.03$ in H_2O, obtaining amphibole with 0.2 wt% Cl, and only obtained amphibole with Cl >0.4 wt% in experiments using fluids above NaCl saturation (i.e. brines). Cl contents of these amphibole products still gradually increased in the range from 0.2 to 0.4 wt% Cl with 15 to 60 wt% NaCl in fluid, and only start to show sharp increases after a fluid NaCl concentration of 85 wt%. Accordingly, data from Khodorevskaya and Aranovich (2016) show little difference in Cl content between amphibole formed in equilibrium with a fluid containing 35 wt% NaCl and amphibole formed in 70 wt% NaCl fluid experiments. This is also the case in our study, where average Cl contents in amphibole are similar in 20 and 50 wt% NaCl experiments. However, even though the maximum Cl content obtained in amphibole in the present study (0.47 wt% Cl) is the same at both 20 and 50wt% fluid NaCl contents, the average Cl contents are significantly higher than those obtained with the lower saline fluid (6 wt% NaCl) (Fig. 9A).

It is hard to determine whether temperature exerts an influence on Cl incorporation in amphibole (Fig. 9B) within the range evaluated (500 °C to 900 °C). Higher fluid/rock ratios – such as in experiments performed at 600 °C and 500 °C at fluid/rock ratios of 1 – have not been found to play a large role on the significant increase in Cl content of the amphibole. The approach of running the reacted rock in a second experiment at the same temperature with a new batch of saline fluid resulted in increased maximum Cl in amphibole for experiments performed with a fluid with 20 wt% NaCl, and 50 wt% Cl at 750 °C, with respect to experiments run only once at the same conditions. However, experiments performed at 650 °C and 900 °C yielded higher maximum Cl contents, thus a better comparison should be made by using the same approach at different temperatures in order to assess the effect of the experimental procedure of reacting the rock with added fluid multiple times, i.e. maintaining high chemical potential gradients relevant for open systems.

5. Concluding remarks

After conducting experiments at 900 °C, 750 °C, 650 °C, 600 °C and 500 °C, at pressures of 200 MPa, we conclude that the reaction of gabbro with a saline fluid using our chosen experimental setup leads to the formation of different amphibole types similar to those occurring in nature in lower oceanic crustal environments due to deep hydrothermal activity. Thus, these experiments successfully simulate fluid/rock interaction processes leading to amphibole formation and alteration occurring in natural environments at a range of conditions from granulite facies down to greenschist facies.

When comparing the results of the different experimental conditions used, there is a clear correlation between extent of hydrothermal activity (fluid/rock ratio) and variability of amphibole compositions, with the narrowest range of compositions produced in suprasolidus experiments (900 °C), and the largest compositional variations produced in experiments at the lowest temperatures (subsolidus conditions: 500 and 600 °C). In addition, Cl-bearing amphibole was formed from a Cl-poor starting amphibole with Cl contents of up to 0.47 wt%. In terms of Cl enrichment in amphibole, fluid saturation in NaCl is the most influential variable on Cl incorporation for the conditions used, and therefore fluid salinity may be one of the main driving forces governing the Cl contents in product amphibole. In terms of structural controls on the incorporation of Cl into amphibole, the comparison of cation variations in our experimental products with those of natural and experimental samples from other studies has shown similarities in the lack of correlation between Cl in amphibole and cations such as Fe^{2+}, ^{IV}Al and K in specimens with Cl wt% < 1.

Acknowledgements

The research leading to these results has received funding from the People Programme (Marie Curie Actions) of the European Union's Seventh Framework Programme FP7/2007-2013/ under REA grant agreement n°608001. Many thanks to L.Aranovich and anonymous reviewer for their comments and suggestions which significantly improved this manuscript. Special thanks go to Chao Zhang and Eric Wolff for helpful discussions, guidance and assistance during EPMA sessions. Thanks also to Julian Feige for thin section and epoxy mount preparation, Ulrich Kroll for technical assistance with CSPV, Harald Behrens and Marize Muniz da Silva for guidance in the operation of the CSPV in Hannover, and Lea Scholten for sample capsule preparation and starting the CSPV experiments in Kiel. We also wish to thank Sören Wilke and André Stechern for assistance in the lab and in operation of IHPVs, and Filippo Ridolfi for helpful discussion and guidance. This research used samples provided by the International Ocean Discovery Program (IODP).

References

Allen, D.E., Seyfried, W.E., 2003. Compositional controls on vent fluids from ultramatic-hosted hydrothermal systems at mid-ocean ridges: an experimental study at 400°C, 500 bars. Geochimica et Cosmochimica Acta 67 (8), 1531–1542.

Alt, J.C., Laverne, C., Coggon, R.M., Teagle, D.A.H., Banerjee, N.R., Morgan, S., Smith-Duque, C.E., Harris, M., Galli, L., 2010. Subsurface structure of a submarine hydrothermal system in ocean crust formed at the East Pacific rise, ODP/IODP Site 1256. Geochemistry Geophysics Geosystems 11 (10).

Aranovich, L., Newton, R., 1996. $_{H2}O$ activity in concentrated NaCl solutions at high pressures and temperatures measured by the brucite-periclase equilibrium. Contributions to Mineralogy and Petrology 125 (2–3), 200–212.

Aranovich, L., Safonov, O., 2018. Halogens in high-grade metamorphism. In: Harlov, D., Aranovich, L. (Eds.), The Role of Halogens in Terrestrial and Extraterrestrial Geochemical Processes. Springer, Cham, pp. 713–757 https://doi.org/10.1007/978-3-319-61667-4_11.

Aranovich, L.Y., Bortnikov, N.S., Serebryakov, N.S., Sharkov, E.V., 2010. Conditions of the formation of plagiogranite from the Markov Trough, Mid-Atlantic Ridge, 5°52′–6°02′N. Doklady Earth Sciences 434, 1257–1262 Part 1.

Berndt, J., Liebske, C., Holtz, F., Freise, M., Nowak, M., Ziegenbein, D., Hurkuck, W., Koepke, J., 2002. A combined rapid-quench and H2-membrane setup for internally heated pressure vessels: Description and application for water solubility in basaltic melts. American Mineralogist 87 (11—12), 1717–1726.

Bosch, D., Jamais, M., Boudier, F., Nicolas, A., 2004. Deep and high-temperature hydrothermal circulation in the Oman Ophiolite - Petrological and Isotopic evidence. Journal of Petrology 45 (6), 1181–1208.

Canales, J.P., Detrick, R.S., Toomey, D.R., Wilcock, W.S.D., 2003. Segment-scale variations in the crustal structure of 150-300 kyr old fast spreading oceanic crust (East Pacific rise, 8 degrees 15 ' N-10 degrees 5 ' N) from wide-angle seismic refraction profiles. Geophysical Journal International 152, 766–794.

Chan, A., Jenkins, D.M., Dyar, M.D., 2016. Partitioning of Chlorine between NaCl Brines and Ferro-Pargasite: Implications for the Formation of Chlorine-Rich Amphiboles in Mafic Rocks. The Canadian Mineralogist 54 (1), 337–351.

Chou, I.M., 1986. Permeability of precious metals to hydrogen at 2kb total pressure and elevated temperatures. American Journal of Science 286 (8), 638–658.

Coogan, L.A., Wilson, R.N., Gillis, K.M., MacLeod, C.J., 2001. Near-solidus evolution of oceanic gabbros: Insights from amphibole geochemistry. Geochimica et Cosmochimica Acta 65 (23), 4339–4357.

Currin, A., Wolff, P.E., Koepke, J., Almeev, R.R., Zhang, C., Zihlmann, B., Ildefonse, B., Teagle, D.A.H., 2018. Chlorine-rich amphibole in deep layered gabbros as evidence for brine/rock interaction in the lower oceanic crust: A case study from the Wadi Wariyah, Samail Ophiolite, Sultanate of Oman. Lithos https://doi.org/10.1016/j.lithos.2018.09.015 ISSN 0024-4937.

Driesner, T., 2007. The System H2O-NaCl. II. Correlations for molar volume, enthalpy, and isobaric heat capacity from 0 to 1000 degrees C, 1 to 5000 bar, and 0 to 1 XNaCl. Geochimica et Cosmochimica Acta 71 (20), 4902–4919.

Driesner, T., Heinrich, C., 2007. The system H2O–NaCl. Part I: Correlation formulae for phase relations in temperature–pressure–composition space from 0 to 1000°C, 0 to 5000bar, and 0 to 1 XNaCl. Geochimica et Cosmochimicha Acta 71 (20), 4880–4901.

Dunn, R.A., Toomey, D.R., Solomon, S.C., 2000. Three-dimensional seismic structure and physical properties of the crust and shallow mantle beneath the East Pacific rise at 9°30′N. Journal of Geophysical Research 105 (B10), 23537–23555.

Enami, M., Liou, J.G., Bird, D.K., 1999. Cl-bearing amphibole in the Salton Sea Geothermal System, California. Canadian Mineralogist 30, 1077–1092.

Erdmann, M., Koepke, J., 2016. Experimental temperature cycling as a powerful tool to enlarge melt pools and crystals at magma storage conditions. American Mineralogist 101 (4), 960–969. https://doi.org/10.2138/am-2016-5398.

Filiberto, J., Treiman, A.H., 2009. Martian magmas contained abundant chlorine, but little water. Geology 37 (12), 1087–1090.

Gillis, K.M., Coogan, L.A., Chaussidon, M., 2003. Volatile element (B, Cl, F) behaviour in the roof of an axial magma chamber from the East Pacific rise. Earth and Planetary Science Letters 213, 447–462.
Grant, T.B., Harlov, D.E., 2018. The influence of NaCl-H2O fluids on reactions between olivine and plagioclase: an experimental study at 0.8 GPa and 800–900°C. Lithos https://doi.org/10.1016/j.lithos.2018.07.013.
Gregory, R.T., Taylor, H.P., 1981. An oxygen isotope profile in a section of cretaceous oceanic crust, Samail Ophiolite, Oman: evidence for δ18O buffering of the oceans by deep (>5 km) seawater-hydrothermal circulation at mid-ocean ridges. Journal of Geophysical Research: Solid Earth 86 (B4), 2737–2755.
Ito, E., Anderson, A.T., 1983. Submarine metamorphism of gabbros from the Mid-Cayman rise: petrographic and mineralogic constraints on hydrothermal processes at low-spreading ridges. Contributions to Mineralogy and Petrology 82, 371–388.
Ito, E., Clayton, R.N., 1983. Submarine metamorphism of gabbros from the Mid-Cayman rise: an oxygen isotopic study. Geochimica et Cosmochimica Acta 47 (3), 535–546.
Jarosewich, E., Nelen, J., Norberg, J.A., 1980. Reference samples for electron microprobe analysis. Geostandards Newsletter 4 (1), 43–47.
Khodorevskaya, L.I., Aranovich, L.Y., 2016. Experimental study of amphibole interaction with H2O–NaCl Fluid at 900°C, 500 MPa: toward granulite facies melting and mass transfer. Journal of Petrology 24 (3), 215–233.
Koepke, J., Feig, S.T., Snow, J., Freise, M., 2004. Petrogenesis of oceanic plagiogranites by partial melting of gabbros: an experimental study. Contributions to Mineralogy and Petrology 146, 414–432.
Koepke, J., Berndt, J., Feig, S.T., Holtz, F., 2007. The formation of SiO2-rich melts within the deep oceanic crust by hydrous partial melting of gabbros. Contributions to Mineralogy and Petrology 153, 67–84.
Koepke, J., Christie, D.M., Dziony, W., Holtz, F., Lattard, D., Maclennan, J., Park, S., Scheibner, B., Yamasaki, T., Yamasaki, S., 2008. Petrography of the Dike/Gabbro Transition at IODP Site 1256D (Equatorial Pacific): The Evolution of the Granoblastic Dikes. Geochemistry Geophysics Geosystems 9.
Koepke, J., France, L., Müller, T., Faure, F., Goetze, N., Dziony, W., Ildefonse, B., 2011. Gabbros from IODP Site 1256 (Equatorial Pacific): Insight into axial magma chamber processes at fast-spreading ocean Ridges. Geochemistry Geophysics Geosystems 12.
Kullerud, K., 1996. Chlorine-rich amphiboles; interplay between amphibole composition and an evolving fluid. European Journal of Mineralogy 8 (2), 355.
Kullerud, K., 2000. Occurrence and origin of Cl-rich amphibole and biotite in the Earth's crust - implications for fluid composition and evolution. In: Stober, I., Bucher, K. (Eds.), Hydrogeology of Crystalline Rocks. Kluwer Academic Publishers, pp. 205–225.
Leake, B.E., Woolley, A.R., Arps, C.E.S., Birch, W.D., Gilbert, M.C., Grice, J.D., Hawthorne, F.C., Kato, A., Kisch, H.J., Krivovichev, V.G., Linthout, K., Laird, J., Mandarino, J., Maresch, W.V., Nickel, E.H., Rock, N.M.S., Schumacher, J.C., Smith, D.C., Stephenson, N.C.N., Ungaretti, L., Whittaker, E.J.W., Youzhi, G., 1997. Nomenclature of amphiboles: Report of the subcommittee on amphiboles of the International Mineralogical Association Commission on New Minerals and Mineral Names. The Canadian Mineralogist 35, 219–246.
Lecuyer, C., Reynard, B., 1996. High-temperature alteration of oceanic gabbros by seawater (Hess deep, Ocean Drilling Program Leg 147): evidence from oxygen isotopes and elemental fluxes. Journal of Geophysical Research: Solid Earth 101 (B7), 15883–15897.
Léger, A., Rebbert, C., Webster, J., 1996. Cl-rich biotite and amphibole from Black Rock Forest, Cornwall, New York. American Mineralogist 81, 495–504.
Liu, J., Liu, W., Ye, K., Mao, Q., 2009. Chlorine-rich amphibole in Yangkou eclogite, Sulu ultrahigh-pressure metamorphic terrane, China. European Journal of Mineralogy 21, 1265–1285.
Locock, A.J., 2014. An Excel spreadsheet to classify chemical analyses of amphiboles following the IMA 2012 recommendations. Computers and Geosciences 62, 1–11.
Maclennan, J., Hulme, T., Singh, S.C., 2005. Cooling of the lower oceanic crust. Geology 33 (5), 357–360. https://doi.org/10.1130/G21207.1.
Makino, K., Tomita, K., 1993. Effect of chlorine on the crystal structure of a chlorine-rich hastingsite. Mineralogical Magazine 57, 677–785.
Manning, C., Weston, P., Mahon, K., 1996. Rapid high temperature metamorphism of East Pacific rise gabbros from Hess Deep. Earth and Planetary Science Letters 144, 123–132.
McCormick, K.A., McDonald, A.M., 1999. Chlorine-bearing amphiboles from the Fraser mine, Sudbury, Ontario, Canada: description and crystal chemistry. The Canadian Mineralogist 37, 1385–1403.
McCulloch, M.T., Gregory, R.T., Wasserburg, G.J., Taylor, H.P., 1981. Sm-Nd, Rb-Sr, and 18O/16O isotopic systematics in an oceanic crustal section: evidence from the Samail Ophiolite. Journal of Geophysical Research: Solid Earth 86 (B4), 2721–2735.
Morrison, J., 1991. Compositional constraints on the incorporation of CI into amphiboles. American Mineralogist 76, 1920–1930.
Mueller, B.L., Jenkins, D.M., Dyar, M.D., 2017. Chlorine incorporation in amphiboles synthesized along the magnesio-hastingsite–hastingsite compositional join. European Journal of Mineralogy 29 (2), 167–180.
Nicolas, A., Mainprice, D., Boudier, F., 2003. High temperature seawater circulation throughout crust of oceanic ridges: A model derived from the Oman ophiolites. J. Geophys. Res. 108 (B8), 2371. https://doi.org/10.1029/2002JB002094.
Oberti, R., Ungaretti, L., Cannillo, E., Hawthorne, F., 1993. The mechanism of Cl incorporation in amphibole. American Mineralogist 78, 746–752.
Pertsev, A.N., Aranovich, L.Y., Prokofiev, V.Y., Bortnikov, N.S., Cipriani, A., Simakin, S.S., Borisovskiy, S.E., 2015. Signatures of Residual Melts, Magmatic and Seawater-Derived Fluids in Oceanic Lower-Crust Gabbro from the Vema Lithospheric Section, Central Atlantic. Journal of Petrology 56, 1069–1088. https://doi.org/10.1093/petrology/egv028.
Pitzer, K.S., Sterner, S.M., 1995. Equations of state valid continuously from zero to extreme pressures with H_2O and CO_2 as examples. International Journal of Thermophysics 16 (2), 511–518.
Robie, R.A., Hemingway, B.S., Fischer, J.R., 1978. Thermodynamic properties of minerals and related subtances at 298.15 K and 1 bar (105 Pascals) pressure and at higher temperature. U.S. Geological Survey Bulletin 1452, 456.
Sato, H., Holtz, F., Behrens, H., Botcharnikov, R., Nakada, S., 2005. Experimental Petrology of the 1991–1995 Unzen Dacite, Japan. Part II: Cl/OH Partitioning between Hornblende and Melt and its Implications for the Origin of Oscillatory Zoning of Hornblende Phenocrysts. Journal of Petrology 46 (2), 339–354. https://doi.org/10.1093/petrology/egh078.
Sautter, V., Jambon, A., Boudouma, O., 2006. Cl-amphibole in the nakhlite MIL 03346: evidence for sediment contamination in a Martian meteorite. Earth and Planetary Science Letters 252 (1), 45–55.
Shaw, H.R., Wones, D.R., 1964. Fugacity coefficients for hydrogen gas between 0° and 1000°C, for pressures to 3000 atm. American Journal of Science 262 (7), 918–929.
Silantyev, S.A., Kostitsyn, Yu.A., Cherkashin, D.V., Dick, H.J.B., Kelemen, P.B., Kononkova, N.N., Kornienko, E.M., 2008. Magmatic and Metamorphic Evolution of the Oceanic Crust in the Western Flank of the MAR Crest Zone at 15° 44' N: Investigation of Cores from Sites 1275B and 1275D, JOIDES Resolution Leg 209. Petrology 16 (4), 353–375.
Silantyev, S.A., Aranovich, L.Y., Bortnikov, N.S., 2010. Oceanic Plagiogranites as a result of Interaction between Magmatic and Hydrothermal Systems in the Slow-Spreading Mid-Ocean Ridges. Petrology 18 (4), 369–383.
Silva, M.M., Holtz, F., Namur, O., 2017. Crystallization experiments in rhyolitic systems: the effect of temperature cycling and starting material on crystal size distribution. American Mineralogist 102, 2284–2294.
Taylor, G.J., Boynton, W.V., McLennan, S.M., Martel, L.M.V., 2010. K and Cl concentrations on the Martian surface determined by the Mars Odyssey Gamma Ray Spectrometer: Implications for bulk halogen abundances in Mars. Geophysica., 2017. Crystallization experiments in rhyolitic systems: the effect of temperature cycling and starting material on crystal size distribution. American Mineralogist 102 (11), 2284–2294.
Vanko, D., 1986. High-chlorine amphiboles from oceanic rocks: product of highly saline hydrothermal fluids. American Mineralogist 71, 51–59.
Volfinger, M., Robert, J.L., Vielzeuf, D., Neiva, A.M.R., 1985. Structural control of the chlorine content of OH-bearing silicates (micas and amphiboles). Geochimica et Cosmochimica Acta 49 (1), 37–48.
Webster, J.D., 1992. Fluid-melt interactions involving Cl-rich granites: Experimental study from 200 to 800 MPa. Geochimica et Cosmochimica Acta 56 (2), 659–678.
Whitney, D.L., Evans, B.W., 2010. Abbreviations for names of rock-forming minerals. American Mineralogist 95, 185–187.
Wolff, P.E., 2014. Hydrothermal Circulation from Very High to Low Temperatures in the Lower Oceanic Crust - Evidence from Layered Gabbros from the Oman Ophiolite and from Partial Melting Experiments on Oceanic Gabbros. PhD Thesis, Leibniz Universität Hannover, p. 167.
Wolff, P.E., Koepke, J., Feig, S.T., 2013. The reaction mechanism of fluid-induced partial melting of gabbro in the oceanic crust. European Journal of Mineralogy 25, 279–298.